Genomic diversity of SARS-CoV-2 can be accelerated by mutations in the nsp14 gene

Kosuke Takada[1,2], Mahoko Takahashi Ueda[3], Shintaro Shichinohe[1] Yurie Kida[1], Chikako Ono[4,5], Yoshiharu Matsuura[4,5], Tokiko Watanabe[1,5,6]* and So Nakagawa[2,7]*.

[1]*Department of Molecular Virology, Research Institute for Microbial Diseases, Osaka University, Suita, Osaka, Japan.*

[2]*Department of Molecular Life Science, Tokai University School of Medicine, Isehara, Kanagawa, Japan.*

[3]*Department of Genomic Function and Diversity, Medical Research Institute, Tokyo Medical and Dental University, Bunkyo, Tokyo, Japan*

[4]*Laboratory of Virus Control, Research Institute for Microbial Diseases, Osaka University, Suita, Osaka, Japan*

[5]*Center for Infectious Disease Education and Research, Osaka University, Suita, Osaka, Japan.*

[6]*Center for Advanced Modalities and DDS, Osaka University, Suita, Osaka, Japan.*

[7]*Bioinformation and DDBJ Center, National Institute of Genetics, Mishima, Shizuoka, Japan.*

*Corresponding author

E-mail: tokikow@biken.osaka-u.ac.jp (Tokiko Watanabe) and so@tokai.ac.jp (So Nakagawa)

ORCID: 0000-0001-6461-5379 (Tokiko Watanabe) and 0000-0003-1760-3839 (So Nakagawa)

Abstract (<150 words)

Coronaviruses, including severe acute respiratory syndrome coronavirus 2 (SARS-CoV-2), encode a proofreading exonuclease, nonstructural protein 14 (nsp14), that helps ensure replication competence at a low evolutionary rate compared with other RNA viruses. In the current pandemic, SARS-CoV-2 has accumulated diverse genomic mutations including in nsp14. Here, to clarify whether amino acid substitutions in nsp14 affect the genomic diversity and evolution of SARS-CoV-2, we searched for amino acid substitutions in nature that may interfere with nsp14 function. We found that viruses carrying a proline-to-leucine change at position 203 (P203L) have a high evolutionary rate and that a recombinant SARS-CoV-2 virus with the P203 mutation acquired more diverse genomic mutations than wild-type virus during its replication in hamsters. Our findings suggest that substitutions, such as P203L, in nsp14 may accelerate the genomic diversity of SARS-CoV-2, contributing to virus evolution during the pandemic.

Keywords

coronavirus, mutation, non-structural protein 14, SARS-CoV-2

Introduction

Virus mutates rapidly, resulting in the increased genetic diversity that drives virus evolution and facilitates virus adaptation. Generally, RNA viruses have a high mutation rate because they replicate their genome by using an error-prone RNA-dependent RNA polymerase (RdRp) so that nucleotide incorporation errors are not corrected (1-3). In contrast, coronaviruses have lower mutation rates because they possess nonstructural protein 14 (nsp14), which contains an exoribonuclease (ExoN) domain that provide a proofreading function (4, 5). Nonetheless, in the case of severe acute respiratory syndrome coronavirus-2 (SARS-CoV-2), which emerged in China at the end of 2019 and caused the COVID-19 pandemic, numerous variants have emerged by acquiring multiple mutations in a short period of time. Some of these variants have been a cause for concern due to their increased infectivity, transmissibility, pathogenicity, and/or reduced sensitivity to vaccines and therapeutic agents. These variants, classified as 'variants of concern (VOCs)' by the World Health Organization (WHO), include Alpha (PANGO ID B.1.1.7), Beta (PANGO ID B.1.351), Gamma (PANGO ID P.1), Delta (PANGO ID B.1.617.2), and most recently Omicron (PANGO ID B.1.1.529). To control COVID-19 and bring the pandemic to an end, it is important to understand the mechanism of the emergence of these diverse variants and the genomic evolution of SARS-CoV-2.

Coronaviruses possess a positive-sense, single-stranded RNA genome that is one of the largest among known RNA viruses, ranging from 26 to 32 kb (2). There are two large open reading frames (ORFs) at the 5′ proximal end, ORF1a and ORF1b, which comprise approximately two-thirds of the genome, and encode two large polyproteins, pp1a and pp1ab, that are cleaved into about 16 nonstructural proteins (nsps). Some of the processed nsps assemble to form the replication-transcription complex, which contains an RdRp (nsp12), the helicase (nsp13), processivity factors (nsp7 and nsp8), and the proofreading ExoN complex (nsp14 and nsp10) (6-8). During genome replication, nsp14 ExoN activity plays a role in the RNA proofreading machinery by efficiently removing mismatched 3'-endnucleotides (9). Experiments in which the nsp14 of

SARS-CoV was functionally inactivated revealed 10–20 times higher mutation rates (5, 10, 11), indicating that nsp14 may be essential for maintaining the virus genome.

In this study, to clarify whether amino acid substitutions in nsp14 affect the genomic diversity and evolution of SARS-CoV-2, we searched for amino acid substitutions in nature that may interfere with the function of nsp14 in SARS-CoV-2. First, to obtain functionally important sites in nsp14, we examined 62 representative coronaviruses belonging to the family *Coronaviridae* and found that 99 of the 527 amino acid sites of nsp14 were evolutionarily conserved. We then examined nsp14 sequences obtained from 28,082 SARS-CoV-2 genomes available in the GISAID EpiCoV database, which includes not only sequencing data but also sampling date, country, and institution information (12), and identified an additional 6 amino acid changes in nsp14 mutants that were not detected in the 62 representative coronaviruses. We examined the genome mutation rates of these mutants and found that substitution of proline (P) for leucine (L) at position 203 of nsp14 increased the nucleotide mutation rate of SARS-CoV-2 genomes. To investigate the biological significance of the nsp14 P203L substitution, we generated recombinant SARS-CoV-2 viruses possessing wild-type nsp14 or mutant nsp14 with P203L and characterized them in a hamster model. We found that the nsp14-P203L mutant grown in the lungs of hamsters acquired significantly more diverse genomic mutations than did the wild-type virus. These results indicate that substitutions in nsp14, such as P203L, could accelerate the genomic diversity of SARS-CoV-2.

Results

Conserved regions of nsp14 proteins among coronaviruses

We first generated a phylogenetic tree of the amino acid sequences of the nsp14 gene obtained from 62 representative coronaviruses (the viruses used in this analysis are summarized in Supplementary Table 1). The phylogenetic tree clearly showed the relationship among the four genera of coronaviruses (Fig. 1), consistent with results obtained by using the partial amino acid sequences of ORF1ab described in a previous report (13). Our results suggest that the nsp14 gene is broadly conserved among coronaviruses, and that the conserved amino acid sites could be important for its molecular function.

Next, we examined the conserved amino acid sites of the nsp14 gene among the 62 coronaviruses (Fig. 2A). The amino acid positions of nsp14 were based on the SARS-CoV three-dimensional structure (PDB ID: 5C8S); SARS-CoV and SARS-CoV-2 both belong to the subgenus *Sarbecovirus* in the genus *Betacoronavirus*. For nsp14, the number of identical amino acids was 482/527 (91.5%) in 8 representative coronaviruses belonging to the subgenus *Sarbecovirus*, and 359/527 (68.1%) if we included the nsp14 of the Bat Hp-betacoronavirus/Zhejiang2013 (GenBank ID: NC_025217.1) belonging to the subgenus *Hibecovirus*, an outgroup of *Sarbecovirus*. Moreover, 200/527 (38.0%) positions were conserved among 29 viruses of the genus *Betacoronavirus*, and 108/527 (20.5%) positions were conserved among the 61 coronaviruses (Fig. 2A). If we included an unclassified coronavirus found in *Tropidophorus sinicus* (Chinese waterside skink) (14), the conserved amino acid positions were 99/527 (18.8%). These results suggest that these amino acid sites of the nsp14 gene are conserved among diverse coronaviruses because they may be functionally important. We further validated this hypothesis by calculating nonsynonymous (dN) and synonymous (dS) substitution rates on a per-site basis for the nsp14 sequences of the 62 coronaviruses by using the SLAC program (see Materials and Methods) (15). Codon position 504 of nsp14 was calculated using 61 coronaviruses (i.e., excluding the Chinese waterside skink

coronavirus because it has a mixed nucleotide at that position). As a result, no positive selection sites were found in nsp14, whereas 379 of the 527 sites were under negative selection ($P < 0.01$, Supplementary Fig. 1). In total, 91 amino acids were unchanged and under negative selection in the nsp14 of the 62 representative coronaviruses.

We then investigated whether the amino acids that are known to be important for the error-correcting function of nsp14 are conserved. Coronavirus nsp14 possesses both ExoN and N7-MTase activities. The ExoN domain of coronavirus nsp14 was originally identified based on its sequence similarity to distant cell homologs (9) and has been assigned to the DEDD exonuclease superfamily, which includes the proofreading domains of many DNA polymerases and other eukaryotic and prokaryotic exonucleases. The nsp14 proteins have four conserved active site residues distributed in three standard motifs of the primary structure: residues 90D/92E (motif I), 191E (motif II), and 273D (motif III) (16, 17). We found that the four active sites of nsp14 were conserved among the 62 coronaviruses examined in this study (Fig. 2B). Moreover, there were three zinc fingers that were essential for nsp14 function: zinc finger 1 (ZF1) comprising 207C, 210C, 226C, and 229H; zinc finger 2 (ZF2) comprising 257H, 261C, 264H, and 279C; and zinc finger 3 (ZF3) comprising 452C, 473C, 484C, and 487H. S-adenosyl methionine (SAM)-binding motif I includes residues 331D, 333G, 335P, and 337A (or 337G), which are involved in the (N7 guanine)-methyl transferase reaction by nsp14. We found that all these residues were conserved among the nsp14 sequences of the 62 coronaviruses examined (Supplementary Fig. 2). These results suggest that the amino acids of nsp14 that are functionally important are conserved among the diversified coronaviruses.

Diversity of nsp14 in SARS-CoV-2

Amino acid comparisons of nsp14 in the 62 representative coronaviruses revealed that several sites are strongly conserved and that some substitutions may have deleterious effects on the

survival of SARS-CoV-2. SARS-CoV-2 was first detected in humans in 2019 and has spread rapidly all over the world in a short period of time. Therefore, some nsp14 mutations that impair its error-correcting function may remain in the SARS-CoV-2 population. Accordingly, we attempted to identify such deleterious mutations in the current SARS-CoV-2 population.

We downloaded the aligned nucleotide sequences of SARS-CoV-2 (87,625 sequences) from the GISAID database as of September 7, 2020. The SARS-CoV-2 genomes isolated from humans were extracted (87,304 sequences), and the sequences containing undetermined and/or mixed nucleotides were removed; the remaining 28,082 sequences were used in subsequent analyses. The coding region of nsp14 was translated and compared. The results showed that 25,913 nsp14 amino acid sequences (92.27%) were identical to that of the reference sequence, whereas 2169 sequences contained at least one amino acid substitution in nsp14 (Supplementary Table 2). The top 20 variants possessing nsp14 with amino acids that were different from the major sequence (shown in Supplementary Fig. 2) are summarized in Table 1. Note that frameshift mutants were excluded from the table because they may affect downstream genes as well. Notably, among the 20 amino acid nsp14 mutants, six amino acids (177F, 377L, 369F, 501I, 203L and 297S) were not found in the 62 nsp14 proteins of the representative coronaviruses (Supplementary Fig. 2).

We further analyzed the evolutionary selection pressures of these 6 amino acid sites by using 73 coronaviruses belonging to the genus *Betacoronaviruses* that includes SARS-CoV-2 (Supplementary Table 3). We confirmed that the six amino acid variants were not found in any of the 73 Beta-coronaviruses (Supplementary Table 3). The six conserved positions (177, 203, 297, 369, 377, and 501) were also found to be under negative selection ($P < 0.01$, Supplementary Table 4). Overall, these results indicate that the conserved amino acid sites of nsp14 are also evolutionarily selected in the genus *Betacoronaviruses*.

Correlation between the amino acid sequences of nsp14 and nucleotide mutation rates in the viral genome

To examine whether the six amino acid substitutions in the nsp14 of SARS-CoV-2 variants affect its proofreading function, we looked for a correlation between the amino acid variants of nsp14 and the genetic diversities of SARS-CoV-2 genomes. The nucleotide mutation rates of SARS-CoV-2 possessing mutated nsp14 were compared to that of SARS-CoV-2 with wild-type nsp14. Sequences for which sampling date information (year, month, and day) was not available were excluded from this analysis. Nucleotide mutations per year were calculated based on the regression coefficient using hCoV-19/Wuhan/Hu-1/2019 (GISAID ID: EPI_ISL_402125) as the reference sequence (see Materials and Methods).

We found that SARS-CoV-2 containing wild-type nsp14 had 19.8 nucleotide mutations in its whole genome per year (Table 2). Conversely, seven SARS-CoV-2 variants containing nsp14 with amino acid substitutions showed 27.3 (L177F), 59.8 (L177F/T372I), 35.9 (P203L), 17.1 (P297S), 26.2 (S369F), 13.0 (F377L), or 21.9 (M501I) nucleotide mutations per year (Fig. 3). Although the substitution rates of the L177F/T372I and F377L variants were found to be unreliable because of limited time ranges, those of the other variants were clearly correlated (Fig. 3). Therefore, SARS-CoV-2 variants possessing nsp14 with the L177F, P203L, S369F, or M501I substitution may have a higher genomic mutation rate than that of SARS-CoV-2 carrying wild-type nsp14.

We further verified the elevated substitution rates found in the various nsp14 mutants. We planned to use all sequences that did not contain any ambiguous nucleotides (shown in Supplementary Table 5) to calculate the evolutionary rates; however, this could cause an overestimation because of sampling biases. Therefore, we extracted representative SARS-CoV-2 genomes by selecting the sequence showing the oldest sampling date if the genome sequences were identical. Using this representative dataset, we analyzed the nucleotide mutations per year of the amino acid substitutions for each site of nsp14 if the amino acid substitutions were present in 20 or

more sequences. Amino acid substitutions caused by frameshifts were excluded. As a result, we evaluated 16 amino acid substitutions in nsp14, and the mean nucleotide mutation rate was 20.7 (Supplementary Fig. 3B). Among these substitutions, we found that the P203L variant of nsp14 (nsp14-P203L) showed the highest mutation rate (35.7 nucleotide mutations per year).

We also evaluated the substitution rates of the seven nsp14 variants for each single cluster in which the maximum number was observed. We assumed that variants were in the same clade if their PANGO IDs (18) and GISAID clades were identical. We found that nsp14-P203L variants in the B.1.1.33 lineage had the highest nucleotide mutation rate (58.8 nucleotide mutations/year) (Supplementary Figs. 4A, 4B and Table 3). Although the number of variants was limited (6), a correlation was clearly observed (Supplementary Fig. 4B and Table 3). In addition, six other nsp-P203L variants in a different cluster (B.1) also showed a relatively high nucleotide mutation rate (28.0 nucleotide mutations/year) (Table 3 and Supplementary Fig. 5). These results indicate that SARS-CoV-2 variants containing nsp14-P203L can accumulate mutations in the viral population.

Mutations in the structural genes of SARS-CoV-2 and validation of substitution rates

Nucleotide mutations in the M and E structural genes have been used to calculate the genome-wide mutation load of SARS-CoV-2, although such mutations may not affect RNA replication (19, 20). Therefore, we also analyzed nucleotide mutations of the structural genes that do not directly interact with viral RNA, that is, the S, M, and E genes. As the number of nucleotide mutations in the E or M gene was only 0 or 1 in most sequences, we summed the number of mutations in all three genes. We found that viruses containing nsp14-L177F or nsp14-P203L had higher rates of nucleotide mutations in the S, M, and E genes per year compared with viruses carrying wild-type nsp14 (Table 2). These results suggest that viruses carrying nsp14-L177F and nsp14-P203L have an increased substitution rate.

To examine whether the substitution rates observed in the nsp14 mutants are high, we calculated the nucleotide mutation rates of the mutants of each structural gene if they were present in 20 or more sequences; 40 mutants including 22, 3, and 5 amino acid substitutions in sites of the S, E, and M genes, respectively, remained. The mean rate of nucleotide mutations per year was 18.4, and its distribution is shown in Supplementary Fig. 3C. We then investigated the possibility that the increase in nucleotide mutation rates observed in the nsp14 gene occurred by chance. We found that the nucleotide mutation rate of nsp14-P203L was in the top 5% of the mutation rates of the mutants examined, although the S-V6F mutant had the largest rate (Supplementary Figs. 3A and 6). However, the elevated nucleotide mutation rate of V6F was found to be due to an outlier sample (shown as a black dot in Supplementary Fig. 6). In fact, if we removed the outlier sample, the nucleotide mutation rate was reduced to 26.2. Conversely, the amino acid substitution rate of nsp14 did not show any extreme bias in the sample. These results suggest that P203L of nsp14 has a higher rate of genomic mutation compared with other amino acid substitutions.

The nsp14-P203L variant in the SARS-CoV-2 population

The nsp14-P203L variants have been isolated from 26 patients mainly in Europe and North America, with the first being reported on March 5, 2020 in The Netherlands (GISAID ID: EPI_ISL_454756, Supplementary Table 5). Considering their PANGO lineages (18) and GISAID clades (shown in Supplementary Table 5), the nsp14-P203L variants appeared at least 10 times. In fact, the nsp14-P203L substitution was observed in both Spike D614 and G614 variants, which have enhanced infection efficiency and have spread worldwide (21). However, we also found that the prevalence of nsp14-P203L variants did not increase steadily over time; the largest number of nsp14-P203L variants found in the B.1.1.33 and B.1 lineages was only six for each (Supplementary Table 5).

The nsp14-P203L mutation effect on protein structure.

To assess the effect of the P203L mutation of nps14, we first investigated the location of residue 203 by using a tertiary structure model of SARS-CoV nsp14 (PDB ID: 5C8S) (22) because the protein structure of SARS-CoV-2 nsp14 is currently not available. Of note, the amino acid residues around position 203 of the nsp14 of SARS-CoV and SARS-CoV-2 are well conserved (Supplementary Fig. 7A). Residue 203 is exposed on the surface of the protein and is in the loop stretching from residues 200 to 214, which is in the interstices of the zinc and magnesium binding sites (positions 207 and 191, respectively, Figs. 4A and 4B). We found that the loop is close to amino acids 1–58, which provides an interaction surface for binding to the co-factor SARS-CoV nsp10 (Supplementary Fig. 7B) (23). The interaction with nsp10 has been shown to greatly increase the nucleolytic activity of SARS-CoV nsp14 (24). Therefore, we investigated the possibility that residues at or around position 203 play an important role in the nsp10-nsp14 interaction. We examined the interaction interface of the SARS-CoV nsp14-nsp10 complex structure (PDB ID: 5C8S) (22) by focusing on residues around position 203. Residues 199–203 (VKIGP) of the nsp14 were identified as part of the interaction interface. However, detailed analysis of the protein complex showed that only residues 200 and 201 bound directly to residues 9 and 21 of nsp10, which are well conserved between SARS-CoV and SARS-CoV-2 (Supplementary Fig. 7A). These results suggest that residue 203 may support binding to nsp10 indirectly by establishing the interaction interface around residues 200 and 201.

Characterization of a recombinant SARS-CoV-2 virus possessing nsp14-P203L *in vitro*.

Genome data analysis suggested that SARS-CoV-2 variants containing nsp14-P203L could accumulate mutations in the viral population. Does the nsp14-P203L amino acid substitution affect viral properties (e.g., increasing the diversity of the viral genome)? To attempt to answer this question, we generated recombinant SARS-CoV-2 (based on hCoV-19/Japan/TY-WK-521/2020)

viruses possessing wild-type nsp14 or P203L nsp14 by using a recently established circular polymerase extension reaction (CPER) method (25). We then we examined the effect of the nsp14-P203L amino acid substitution on the biological properties of SARS-CoV-2.

To determine whether the nsp14-P203L amino acid substitution affects the viral growth efficiency in cultured cells, we examined viral replication efficiency in VeroE6/TMPRSS2 cells. We found that both wild-type virus and nsp14-P203L viruses grew well, with max titers (mean titers = 7.35 log unit and 7.01 log unit, respectively) at 36 h post-infection (Fig. 5A), although the titer of the wild-type virus at 24 h post-infection was slightly higher than that of the nsp14-P203L virus (Fig. 5A).

Next, we analyzed the genomic diversity of the recombinant virus grown in the cultured cells. Three plaque-purified wild-type or nsp14-P203L virus clones were used to infect VeroE6/TMPRSS2 cells, and the genomes of the viruses in the supernatant were collected 48 h later and analyzed by RNA sequencing. Mutations with a read depth of at least 1000 times and an allele frequency of at least 0.5% were compared between the wild-type and nsp14-P203L mutant viruses. The nsp14-P203L mutant grown in VeroE6/TMPRSS2 had 51.33 (±10.96) mutations and the wild-type virus had 46.33 (±9.46) mutations, which was not significantly different (P = 0.65) (Fig. 5B). These results suggest that nsp14-P203L allows efficient virus replication and may not affect viral genome mutagenesis in culture cells.

Biological properties of the recombinant nsp14-P203L virus *in vivo*.

Next, to examine whether the nsp14-P203L amino acid substitution affects viral properties *in vivo* (e.g., increasing viral replication efficiency and/or viral genome diversity), we investigated the biological properties of the nsp14-P203L mutant in a hamster model (Fig. 6A). We inoculated the hamsters intranasally with 10^3 PFU of wild-type virus or virus possessing nsp14-P203L and collected lung and nasal turbinate samples at 3 and 6 days post-infection (dpi) to analyze viral titers

(Fig. 6B). We found that the nsp14-P203L virus replicated well in both the lungs and nasal turbinates of the infected hamsters at 3 and 6 dpi, and the viral titers in the lungs of the hamsters infected with the nsp14-P203L virus at 3 dpi were similar to those in the lungs of the hamsters infected with the wild-type virus (mean titers were 8.38 log unit or 8.33 log unit, respectively). We also observed clinical symptoms, including weight loss for 6 days post-infection. We found that hamsters infected with the nsp14-P203L virus showed similar weight loss to hamsters infected with the wild-type virus (Fig. 6C). The nsp14-P203L mutant virus thus grew as efficiently as the wild-type virus in hamster lungs and nasal turbinate and caused similar weight loss.

To further investigate the effect of nsp14-P203L on viral genome diversity *in vivo*, we RNA-sequenced viral genomes extracted from viruses isolated from the lungs of hamsters infected with the nsp14-P203L or wild-type virus at 6 dpi. We found that the number of mutations in the nsp14-P203L group was significantly higher than those detected in the wild-type group (63.25±12.54 mutations *versus* 32.75±3.34 mutations, respectively; P = 0.0066) (Fig. 6D), and that these mutations were widely distributed in the viral genomes (Fig. 6E). These results indicate that the nsp14-P203L virus replicates well in the respiratory tracts of hamsters and readily acquires more diverse mutations.

Discussion

The mutation rate of coronaviruses, including SARS-CoV-2, is relatively low compared to other RNA viruses because coronaviruses possess an error-correcting exonuclease, nsp14. In this study, we examined mutations that occurred in nsp14, and found that SARS-CoV-2 possessing nsp14 with a proline to leucine substitution at position 203 showed a relatively higher substitution rate (35.9 substitutions/year) than SARS-CoV-2 possessing wild-type nsp14 (19.8 substitutions/year). Moreover, we demonstrated that a recombinant SARS-CoV-2 possessing this P203L substitution in nsp14 acquired significantly more diverse genomic mutations than the wild-type virus did during its replication in a hamster model, suggesting that mutations in nsp14, such as P203L, could accelerate the genomic diversity of SARS-CoV-2.

The frequency of nucleotide mutations of coronaviruses may be affected not only by the nsp14 proofreading mechanism but also by the characteristics of other proteins, such as the fidelity of the RNA-dependent RNA polymerase (nonstructural protein 12; nsp12) (26). The proofreading activity of nsp14 is known to be affected by an amino acid substitution in nsp10, which contributes to its interaction with nsp14 (24). *In silico* analysis of the SARS-CoV nsp14-nsp10 complex suggests that the amino acid residue at position 203 of nsp14 could be important for the interaction with nsp10, which occurs in a region comprising amino acids that are well conserved between SARS-CoV-2 and SARS-CoV (Supplementary Fig. 7A). The nsp14-P203L mutants appeared to weakly interact with nsp10 (Supplementary Figs. 7C and 7D), possibly resulting in a reduction in the proofreading activity of nsp14. In addition, it is possible that amino acid substitutions in other proteins involved in genome replication affect the nucleotide mutation rates of SARS-CoV-2. Therefore, we examined amino acid substitutions among nsp14-203L variants involving the following genes that participate in gene replication: nsp7, nsp8, nsp9, nsp10, nsp12, nsp13, nsp15, and nsp16. The results showed that a proline-to-leucine substitution at position 323 (P323L) of nsp12 frequently occurred (20/25) in sequences of SARS-CoV-2 possessing nsp14-203L (Supplementary Table 6). However, the P323L

mutation in nsp12 (nsp12-P323L) is known to accompany an aspartate-to-glycine substitution at position 614 (D614G) of S protein (21, 27). The S-D614G mutant was first reported at the end of January 2020 in China and Germany, and by March 2020, this mutant was a major variant in various regions all over the world (21). The P323L mutation in nsp12 was found in nsp14-203L variants as well. Indeed, the genomic mutation rate of SARS-CoV-2 with the P323L amino acid substitution in nsp12, was found to be 17.7 nucleotide mutations per year (Supplementary Fig. 8). Therefore, it is unlikely that P323L in nsp12 directly affects the genomic mutation rate of SARS-CoV-2 viruses carrying the P203L amino acid substitution in nsp14.

Alanine substitution of an amino acid that is important for the proofreading activity of the nsp14 of SARS-CoV has been shown to increase viral genomic mutations in cultured cells (5, 11) and *in vivo* (10). In addition, Graham et al. reported that SARS-CoV is also attenuated by such a substitution (10). The effects of amino acid substitutions in nsp14 on coronavirus infections in nature have not been investigated. In our study, candidates that might affect nsp14 function were sought by focusing on amino acid substitutions in the nsp14 of epidemic viruses and comparing genomic mutation rates. However, the molecular mechanism of how amino acid mutations in nsp14 are involved in proofreading activity is not clear. In addition, the number of nsp14 variants, including nsp14-203L variants, was limited in our study, which limited our statistical analysis. Nevertheless, our findings demonstrate that rare amino acid substitutions (particularly leucine at amino acid 203) in coronavirus nsp14 may increase the rate of genomic mutations.

References

1. Sjaarda CP, Guthrie JL, Mubareka S, Simpson JT, Hamelin B, Wong H, et al. Temporal Dynamics and Evolution of SARS-CoV-2 Demonstrate the Necessity of Ongoing Viral Genome Sequencing in Ontario, Canada. mSphere. 2021;6(3).
2. Gorbalenya AE, Enjuanes L, Ziebuhr J, Snijder EJ. Nidovirales: evolving the largest RNA virus genome. Virus Res. 2006;117(1):17-37.
3. Robson F, Khan KS, Le TK, Paris C, Demirbag S, Barfuss P, et al. Coronavirus RNA Proofreading: Molecular Basis and Therapeutic Targeting. Mol Cell. 2020;79(5):710-27.
4. Eckerle LD, Lu X, Sperry SM, Choi L, Denison MR. High fidelity of murine hepatitis virus replication is decreased in nsp14 exoribonuclease mutants. J Virol. 2007;81(22):12135-44.
5. Eckerle LD, Becker MM, Halpin RA, Li K, Venter E, Lu X, et al. Infidelity of SARS-CoV Nsp14-exonuclease mutant virus replication is revealed by complete genome sequencing. PLoS Pathog. 2010;6(5):e1000896.
6. Sola I, Almazan F, Zuniga S, Enjuanes L. Continuous and Discontinuous RNA Synthesis in Coronaviruses. Annu Rev Virol. 2015;2(1):265-88.
7. te Velthuis AJ, van den Worm SH, Snijder EJ. The SARS-coronavirus nsp7+nsp8 complex is a unique multimeric RNA polymerase capable of both de novo initiation and primer extension. Nucleic Acids Res. 2012;40(4):1737-47.
8. Ahn DG, Choi JK, Taylor DR, Oh JW. Biochemical characterization of a recombinant SARS coronavirus nsp12 RNA-dependent RNA polymerase capable of copying viral RNA templates. Arch Virol. 2012;157(11):2095-104.
9. Snijder EJ, Bredenbeek PJ, Dobbe JC, Thiel V, Ziebuhr J, Poon LLM, et al. Unique and Conserved Features of Genome and Proteome of SARS-coronavirus, an Early Split-off From the Coronavirus Group 2 Lineage. Journal of Molecular Biology. 2003;331(5):991-1004.
10. Graham RL, Becker MM, Eckerle LD, Bolles M, Denison MR, Baric RS. A live, impaired-fidelity coronavirus vaccine protects in an aged, immunocompromised mouse model of lethal disease. Nat Med. 2012;18(12):1820-6.
11. Smith EC, Blanc H, Surdel MC, Vignuzzi M, Denison MR. Coronaviruses lacking exoribonuclease activity are susceptible to lethal mutagenesis: evidence for proofreading and potential therapeutics. PLoS Pathog. 2013;9(8):e1003565.
12. Shu Y, McCauley J. GISAID: Global initiative on sharing all influenza data - from vision to reality. Euro Surveill. 2017;22(13).
13. Nakagawa S, Miyazawa T. Genome evolution of SARS-CoV-2 and its virological characteristics. Inflamm Regen. 2020;40:17.
14. Shi M, Lin XD, Chen X, Tian JH, Chen LJ, Li K, et al. The evolutionary history of vertebrate RNA viruses. Nature. 2018;556(7700):197-202.

15. Kosakovsky Pond SL, Frost SD. Not so different after all: a comparison of methods for detecting amino acid sites under selection. Mol Biol Evol. 2005;22(5):1208-22.
16. Ogando NS, Ferron F, Decroly E, Canard B, Posthuma CC, Snijder EJ. The Curious Case of the Nidovirus Exoribonuclease: Its Role in RNA Synthesis and Replication Fidelity. Front Microbiol. 2019;10:1813.
17. Romano M, Ruggiero A, Squeglia F, Maga G, Berisio R. A Structural View of SARS-CoV-2 RNA Replication Machinery: RNA Synthesis, Proofreading and Final Capping. Cells. 2020;9(5).
18. Rambaut A, Holmes EC, O'Toole A, Hill V, McCrone JT, Ruis C, et al. A dynamic nomenclature proposal for SARS-CoV-2 lineages to assist genomic epidemiology. Nat Microbiol. 2020;5(11):1403-7.
19. Eskier D, Karakulah G, Suner A, Oktay Y. RdRp mutations are associated with SARS-CoV-2 genome evolution. PeerJ. 2020;8:e9587.
20. Eskier D, Suner A, Oktay Y, Karakulah G. Mutations of SARS-CoV-2 nsp14 exhibit strong association with increased genome-wide mutation load. PeerJ. 2020;8:e10181.
21. Korber B, Fischer WM, Gnanakaran S, Yoon H, Theiler J, Abfalterer W, et al. Tracking Changes in SARS-CoV-2 Spike: Evidence that D614G Increases Infectivity of the COVID-19 Virus. Cell. 2020;182(4):812-27 e19.
22. Ma Y, Wu L, Shaw N, Gao Y, Wang J, Sun Y, et al. Structural basis and functional analysis of the SARS coronavirus nsp14-nsp10 complex. Proc Natl Acad Sci U S A. 2015;112(30):9436-41.
23. Ogando NS, Zevenhoven-Dobbe JC, van der Meer Y, Bredenbeek PJ, Posthuma CC, Snijder EJ. The Enzymatic Activity of the nsp14 Exoribonuclease Is Critical for Replication of MERS-CoV and SARS-CoV-2. J Virol. 2020;94(23).
24. Bouvet M, Imbert I, Subissi L, Gluais L, Canard B, Decroly E. RNA 3'-end mismatch excision by the severe acute respiratory syndrome coronavirus nonstructural protein nsp10/nsp14 exoribonuclease complex. Proc Natl Acad Sci U S A. 2012;109(24):9372-7.
25. Torii S, Ono C, Suzuki R, Morioka Y, Anzai I, Fauzyah Y, et al. Establishment of a reverse genetics system for SARS-CoV-2 using circular polymerase extension reaction. Cell Rep. 2021;35(3):109014.
26. Graepel KW, Lu X, Case JB, Sexton NR, Smith EC, Denison MR. Proofreading-Deficient Coronaviruses Adapt for Increased Fitness over Long-Term Passage without Reversion of Exoribonuclease-Inactivating Mutations. mBio. 2017;8(6).
27. Hou YJ, Chiba S, Halfmann P, Ehre C, Kuroda M, Dinnon KH, et al. SARS-CoV-2 D614G Variant Exhibits Enhanced Replication ex vivo and Earlier Transmission in vivo. bioRxiv. 2020.
28. Katoh K, Standley DM. MAFFT multiple sequence alignment software version 7: improvements in performance and usability. Mol Biol Evol. 2013;30(4):772-80.

29. Crooks GE, Hon G, Chandonia JM, Brenner SE. WebLogo: a sequence logo generator. Genome Res. 2004;14(6):1188-90.
30. Darriba D, Taboada GL, Doallo R, Posada D. ProtTest 3: fast selection of best-fit models of protein evolution. Bioinformatics. 2011;27(8):1164-5.
31. Kozlov AM, Darriba D, Flouri T, Morel B, Stamatakis A, Wren J. RAxML-NG: a fast, scalable and user-friendly tool for maximum likelihood phylogenetic inference. Bioinformatics. 2019;35(21):4453-5.
32. Lanave C, Preparata G, Saccone C, Serio G. A new method for calculating evolutionary substitution rates. J Mol Evol. 1984;20(1):86-93.
33. Li W, Godzik A. Cd-hit: a fast program for clustering and comparing large sets of protein or nucleotide sequences. Bioinformatics. 2006;22(13):1658-9.
34. Darriba D, Posada D, Kozlov AM, Stamatakis A, Morel B, Flouri T. ModelTest-NG: A New and Scalable Tool for the Selection of DNA and Protein Evolutionary Models. Mol Biol Evol. 2020;37(1):291-4.
35. Kumar S, Stecher G, Li M, Knyaz C, Tamura K. MEGA X: Molecular Evolutionary Genetics Analysis across Computing Platforms. Mol Biol Evol. 2018;35(6):1547-9.
36. Abascal F, Zardoya R, Telford MJ. TranslatorX: multiple alignment of nucleotide sequences guided by amino acid translations. Nucleic Acids Res. 2010;38(Web Server issue):W7-13.
37. Weaver S, Shank SD, Spielman SJ, Li M, Muse SV, Kosakovsky Pond SL. Datamonkey 2.0: A Modern Web Application for Characterizing Selective and Other Evolutionary Processes. Mol Biol Evol. 2018;35(3):773-7.
38. Martin M. Cutadapt removes adapter sequences from high-throughput sequencing reads. EMBnetjournal. 2011;17(1):3.
39. Li H, Durbin R. Fast and accurate short read alignment with Burrows-Wheeler transform. Bioinformatics. 2009;25(14):1754-60.
40. McKenna A, Hanna M, Banks E, Sivachenko A, Cibulskis K, Kernytsky A, et al. The Genome Analysis Toolkit: a MapReduce framework for analyzing next-generation DNA sequencing data. Genome Res. 2010;20(9):1297-303.
41. Dehouck Y, Kwasigroch JM, Rooman M, Gilis D. BeAtMuSiC: Prediction of changes in protein-protein binding affinity on mutations. Nucleic Acids Res. 2013;41(Web Server issue):W333-9.

Methods

Coronavirus sequence data.

The amino acid sequences of open reading frame 1ab (ORF1ab) of the 62 representative coronaviruses (summarized in Supplementary Table 1) were obtained from NCBI (https://www.ncbi.nlm.nih.gov/) and the GISAID EpiCoV database (https://www.gisaid.org) as reported previously (13). Aligned nucleotide sequences of SARS-CoV-2 and their metadata were obtained from the GISAID EpiCoV database as of September 7, 2020 (87,625 sequences). The coronavirus genome sequences annotated as having "Human" hosts were extracted, and sequences containing undetermined and/or mixed nucleotides were removed. The 28,082 remaining genomes were used for the analyses. The open reading frame (ORF) of each sequence was determined from the alignment sequence based on the ORF information of hCoV-19/Wuhan/Hu-1/2019 (GISAID ID: EPI_ISL_402125, GenBank ID: NC_045512.2), which was used as the reference sequence. Gap sites were removed, and the nucleotide sequences were translated. To detect amino acid substitutions for each site, the amino acid sequence after the stop codon was removed and amino acid sequences were aligned by using the L-INS-i program in MAFFT version v7.453 (28). From the sequence alignment of the nsp14 of the representative coronaviruses, the amino acids aligned at the amino acid positions of SARS-CoV-2 are shown using WebLogo 3 (29). Note that, in the alignment sequence, gap sites were removed based on the SARS-CoV-2 nsp14 sequence.

Molecular evolutionary phylogenetic analysis.

To compute the phylogenetic tree of the nsp14 of the 62 representative coronaviruses, their nsp14 amino acid sequences were aligned by using the L-INS-i program in MAFFT version 7.453 (28). To estimate the appropriate amino acid substitution model, we used ProtTest3 version 3.4.2 (30) based on the Bayesian information criterion (BIC) values. We then computed a phylogenetic tree by using RAxML-NG version 1.0.0 (31) with rapid 1000 bootstrap replicates (32).

We also generated a phylogenetic tree of SARS-CoV-2 genomes belonging to the PANGO lineage B.1.1.33 including nsp14-P203L variants. Using CD-HIT-EST version 4.8.1 (33), identical genomic sequences were removed: from 200 to 142 sequences. The 142 nucleotide sequences were aligned by using the L-INS-i program in MAFFT version 7.453 (28). To estimate the appropriate nucleotide mutation model, we used ModelTest-NG (34) based on the Akaike information criterion (AIC) values, and GTR+I+G4 was selected. We then computed a phylogenetic tree by using RAxML-NG version 1.0.0 (31) with rapid 1000 bootstrap replicates (32).

Substitution rate analysis.

A multiple sequence alignment of SARS-CoV-2 genomes obtained from the GISAID database was used to analyze the genomic evolutionary rate. The number of nucleotide mutations per site from between sequences was counted. Analyses were conducted using the Kimura 2-parameter model. Codon positions included 1st+2nd+3rd+Noncoding. All gaps were removed for each sequence pair with a pairwise deletion option. The number of nucleotide mutations was counted in MEGA X (35). The hCoV-19/Wuhan/Hu-1/2019 (GISAID ID: EPI_ISL_402125, GenBank ID: NC_045512.2) was selected as the reference sequence. Sequences with information that included the collection date were used for the analysis. Note that we omitted sequences that were collected before December 26, 2019, the date on which the reference sequences were collected. The approximate straight line was calculated by using the least-squares method and in-house python scripts.

Measurement of natural selection pressure.

TranslatorX (36) was used to align the nucleotide sequences based on the aligned amino acid sequences of the nsp14 of the representative coronaviruses. To determine the evolutionary selection pressures on the nsp14 gene in coronaviruses, we computed the ratio of nonsynonymous

substitution rates (dN) and synonymous substitution rates (dS) per site (dN/dS) by using Datamonkey software (15, 37) through MEGA X (35).

Cells.

VeroE6/TMPRSS2 (JCRB 1819) cells were maintained in Dulbecco's Modified Eagle Medium (DMEM) supplemented with 10% FBS, 1% Penicillin-Streptomycin Solution, and 1 mg/ml geneticin (G418; Nacalai Tesque, Cat# 09380-44). HEK293-hACE2/hTMPRSS2 cells were maintained in DMEM supplemented with 10% FBS and 1% Penicillin-Streptomycin Solution. VeroE6/TMPRSS2 and HEK293-hACE2/hTMPRSS2 cells were maintained at 37□ with 5% CO_2.

Reverse genetics

Recombinant SARS-CoV-2 was generated by using circular polymerase extension reaction (CPER) as previously described (25). Briefly, nine DNA fragments encoding the partial genome of SARS-CoV-2 (hCoV-19/Japan/TY-WK-521/2020) were amplified by PCR using PrimeSTAR GXL DNA polymerase (Takara, Cat# R050A). A linker fragment encoding the hepatitis delta virus ribozyme, the bovine growth hormone poly A signal, and the cytomegalovirus promoter was also amplified by PCR. The ten DNA fragments were mixed and used for CPER (25).

To produce recombinant SARS-CoV-2 (seed virus), the CPER products were transfected into HEK293-hACE2/hTMPRSS2 cells by using TransIT-LT1 (Takara, Cat# MIR2305). At one day post-transfection, the culture medium was replaced with DMEM (high glucose) (Nacalai Tesque, Cat# 08459-64) containing 2% FBS and 1% Penicillin-Streptomycin Solution. At 4–10 days post-transfection, the culture medium was collected and stock at -80□. The viruses were used to inoculate VeroE6/TMPRSS2 cells to produce stock viruses. No mutations were found in the wild-type viruses, whereas the nsp14-P203L viruses were found to contain mixed unexpected mutations such as C12119T/C (nsp8-P10S/P) and C17143T/C (nsp13-R303C/R). To obtain viruses

with the single mutation of nsp14-P203L, a plaque-purified virus clone was grown in VeroE6/TMPRSS2 cells. All experiments with transfectants generated by reverse genetics were performed in an enhanced biosafety level 3 (BSL3) containment laboratory approved for such used by Osaka university.

Deep sequencing analysis.

Viral RNA was extracted from samples by using the QIAamp Viral RNA Mini kit (Qiagen) according to the manufacturer's instructions. The extracted RNA was reverse transcribed with ProtoScript II (NEB) using N6 primers. The cDNA was converted to double-stranded DNA by NEBNext Second Strand Synthesis (NEB). In addition, double-stranded DNA was fragmented by the SureSelect Fragmentation Enzyme. Fragmented DNA was made into an NGS library with the SureSelect XT Low Input Kit. In addition, hybridization was performed using a SARS-CoV-2 custom probe, and sequence-ready libraries were sequenced in a paired-end run using by MiSeq (Illumina).

The raw FASTQ format data files that were obtained from the sequencing samples were filtered using cutadapt version 3.2 (38) to remove low-quality reads and adapters. Then, the filtered sequences were mapped into the reference SARS-CoV-2 genome (Wuhan-Hu-1, NC_045512.2) by using BWA version 0.7,17-r1188(39). Variant calling was done using MuTect2 in GATK suite version 4.2 (40), and nucleotide changes were counted by using in-house python scripts.

Animal experiments and approvals.

All animal experiments were approved by the Animal Research Committee of the Research Institute for Microbial Diseases, Osaka University (assurance number, R03-04-0). All animals were housed under specific pathogen-free conditions in a temperature and humidity control environment with a 12 h:12 h light dark cycle and ad libitum access to water and standard laboratory chow. Virus

inoculations were performed under anesthesia, and all efforts were made to minimize animal suffering. These *in vivo* studies were not blinded, and animals were randomly assigned to infection groups. No sample-size calculations were performed to power each study. Instead, sample size was determined based on prior *in vivo* virus challenge experiments.

Experimental infection of Syrian hamsters.

Seven-week-old male wild-type Syrian hamsters (Japan SLC Inc., Shizuoka, Japan) were used in this study. Baseline body weights were measured before infection. Under isoflurane anesthesia, four hamsters per group were intranasally inoculated with 10^3 PFU in 30 μl of recombinant virus. Body weight was monitored daily for 6 days after infection. For virological examinations, four hamster per group were intranasally infected with recombinant viruses; 3 and 6 dpi, the animals were euthanized, and nasal turbinate and lungs were collected. The virus titers in the nasal turbinate, trachea and lungs were determined by performing plaque assays on VeroE6/TMPRSS2 cells.

***In silico* structural analysis.**

A PDB file (5C8S) of the SARS-CoV nsp14-nsp10 complex was obtained from the PDB database (https://www.rcsb.org). Using chains C and D of the structure, further analyses were performed. The residues at the interface of the SARS-CoV nsp10-nsp14 docked complex were determined using the "InterfaceResidues" PyMol script (http://www.pymolwiki.org/index.php/InterfaceResidues/). We used the SARS-CoV nsp10-nsp14 docked complex to predict the effect of the P203L mutation on protein-protein interactions by using the BeAtMuSiC program version 1.0 (http://babylone.3bio.ulb.ac.be/beatmusic/query.php) (41). P203L mutant generation, hydrophobicity calculation, and visualization were performed using Discovery Studio Visualizer software.

Statistical analysis.

All data were analyzed in GraphPad Prism software (version 9.4.0). Statistical analysis included ANOVA with multiple corrections, post-tests, or an unpaired Student's t test. Differences among groups were considered significant for P values < 0.05.

Acknowledgments

We thank Dr. Susan Watson for scientific editing. We acknowledge the NGS Core laboratory, Genome Information Research Center, Institute for Microbial Diseases, Osaka University, for assistance with the RNA sequence. We thank the GISAID database (https://www.gisaid.org), which shares sequence data of SARS-CoV-2 and related viral species. This study was supported by KAKENHI Grants-in-Aid for Scientific Research on Innovative Areas 16H06429 (to T.W. and S.N.), 16K21723 (to T.W. and S.N.), 16H06434 (to T.W), and 19H04843 (to S.N.); Grants-in-Aid for Scientific Research (B) JP22H02521 (to T.W.) and JP21H02736 (to C.O); Grant-in-Aid for Early-Career Scientists 22K15469 (to K.T.); Grant-in-Aid for JSPS Fellows 21J01036 (to K.T.); Grants-in-Aid for Scientific Research on Innovative Areas from the Ministry of Education, Culture, Sports, Science, and Technology (MEXT) of Japan JP16H06429 (to Y.M.), JP16K21723 (to Y.M.), and JP16H06432 (to Y.M.); AMED Research Program on Emerging and Re-emerging Infectious Diseases JP20fk0108281 (to Y.M.), JP19fk0108113 (to Y.M. and to T.W.), JP20fk0108401 (to C.O.), JP21fk0108493 (to C.O.), JP19fk018113 (to T.W.) and 19fk0108171 (to S.N.); AMED Cyclic Innovation for Clinical Empowerment (CiCLE) JP20pc0101047 (to Y. M.); AMED under Grant Number JP223fa627002h (to T.W.); AMED Advanced Research and Development Programs for Medical Innovation (AMED-CREST) 22gm1610010h0001 (to T.W.); 2020 Tokai University School of Medicine Research Aid (to S.N.); Japan Science and Technology Agency (JST) Moonshot R&D JPMJMS2025 (to Y.M.); the Tokyo Biochemical Research Foundation (to T.W.); the Takeda Science Foundation (to T.W.); and RIKAKEN HOLDINGS CO. Young Researcher Support Grant-in-aid (to K.T.). The super-computing resources were provided by the Human Genome Center (the Univ. of Tokyo) and the NIG supercomputer at ROIS National Institute of Genetics.

Author information

Affiliations

Department of Molecular Virology, Research Institute for Microbial Diseases, Osaka University, Osaka, Japan.

Kosuke Takada, Shintaro Shichinohe, Yurie Kida and Tokiko Watanabe.

Department of Molecular Life Science, Tokai University School of Medicine, Isehara, Kanagawa, Japan.

Kosuke Takada and So Nakagawa.

Department of Genomic Function and Diversity, Medical Research Institute, Tokyo Medical and Dental University, Bunkyo, Tokyo, Japan

Mahoko Takahashi Ueda.

Laboratory of Virus Control, Research Institute for Microbial Diseases, Osaka University, Suita, Osaka, Japan

Chikako Ono and Yoshiharu Matsuura

Center for Infectious Disease Education and Research, Osaka University, Suita, Osaka, Japan.

Chikako Ono, Yoshiharu Matsuura and Tokiko Watanabe.

Center for Advanced Modalities and DDS, Osaka University, Osaka, Japan.

Tokiko Watanabe.

Contributions

K.T., T.W. and S.N. conceived the study. K.T., M.T.U and S.N analyzed data. C.O. and Y.M. established 293-hACE2/hTMPRSS2 cells. K.T. generated recombinant viruses. K.T. and Y.K. performed in vitro experiments. K.T., S.S. and T.W. performed animal experiments. K.T, M.T.U., T.W and S.N. wrote the manuscript. All authors read and approved the final manuscript.

Competing interests

The authors have no competing interests.

Data Availability Statements

The data underlying this article will be shared upon reasonable request to the corresponding author. All RNA-seq data sequenced in this study were deposited in DDBJ Sequence Read Archive (DRA) with the following accession numbers: DRR411740 - DRR411753

Corresponding authors

Correspondence to Tokiko Watanabe <tokikow@biken.osaka-u.ac.jp> and So Nakagawa <so@tokai.ac.jp>

Figure Legends

Fig. 1: Phylogenetic tree of nsp14

Maximum likelihood (ML)-based phylogenetic tree of the 62 representative coronaviruses. Amino acid sequences of nsp14 in ORF1ab were used for this analysis. A red or blue circle in an internal node corresponds to bootstrap values ≥ 95% or ≥ 80 %, respectively. The virus located at the top is SARS-CoV-2 (hCoV-19/Wuhan/Hu-1/2019).

Fig. 2: Amino acid sequence alignment of nsp14 derived from representative coronaviruses

(A) Conserved amino acid residues among each group. The amino acid sequence of the nsp14 of the 62 representative coronaviruses is shown according to the relative amino acid positions of SARS-CoV-2 nsp14 (note that the gaps in the SARS-CoV-2 sequence are not shown). The conserved amino acid positions are indicated in gray. (B) Four conserved active site residues involved in proofreading. The amino acid proportions for each site were calculated based on the sequence alignment of the nsp14 of the 62 representative coronaviruses visualized by using WebLogo (29).

Fig. 3: Scatter plot of nucleotide mutations in SARS-CoV-2 genomes

Genome diversity of SARS-CoV-2 containing wild-type (WT) nsp14 and 7 nsp14 mutants is shown. The X-axis indicates the sampling date and the Y-axis indicates the number of nucleotide mutations in the genomes. The dotted line corresponds to the regression line.

Fig. 4: Three-dimensional position of the amino acid at position 203 in nsp14

(A) Domain structure of nsp14 with residue numbers. The interaction surface with nsp10 is indicated by the hatched box. The ExoN and N7-Mtase domains are shown in light blue and gray, respectively. The loop from positions 200 to 214 is marked by a dark gray bar. The amino acid at position 203 in

nsp14 is shown in magenta. The amino acid positions of magnesium binding (191), nsp10 binding (200 and 201), and zinc binding (207 and 210) in nsp14 are shown in purple, light pink, and orange, respectively. (B) Schematic representation of nsp14. The coloring is the same as in (A).

Fig. 5: Growth efficiency and genomic mutations of nsp14-P203L variants in cultured cells. (A) Growth kinetics of recombinant viruses in VeroE6/TMPRSS2 cells. VeroE6/TMPRSS2 cells were infected with viruses at a multiplicity of infection of 0.001. The supernatants of the infected cells were harvested at the indicated times, and virus titers were determined by the using plaque assays in VeroE6/TMPRSS2 cells. Data are shown as the mean of three independent experiments done in triplicate. Error bars indicate the standard deviation. Mean values were compared by using a two-way ANOVA, followed by Dunnett's test (*P<0.05). Asterisks indicate statistically significant differences between WT and Mut viruses. (B) Number of genomic mutation types detected in viruses grown in VeroE6/TMPRSS2 cells. Three wild-type or mutant viruses were each plaque-purified, and each viral clone was infected into VeroE6/TMPRSS2 cells; supernatants were collected after 48 hours. RNA was extracted from the virus in the supernatant and RNA sequencing was performed. Mutations with a read depth of at least 1000x and an allele frequency of at least 0.5% were compared between the wild-type and mutant viruses. Mean values were compared by using an unpaired Student's t test (N.D.; P>0.05).

Fig. 6: Growth efficiency and genomic mutations of nsp14-P203L variants in Syrian hamsters. (A) Schematic overview of the animal experiment. Syrian hamsters were inoculated with 10^3 PFU of wild-type or nsp14-P203L virus via the intranasal (30 μL) route. (B) Virus replication in infected Syrian hamsters. Four Syrian hamsters per group were killed on days 3 and 6 post-infection for virus titration. Virus titers in lung or nasal turbinate (NT) organs were determined by using plaque assays in VeroE6/TMPRSS2 cells. Error bars indicate the standard deviation. Mean values were compared

by using a two-way ANOVA, followed by Dunnett's test. (C) Body weight changes in Syrian hamsters after viral infection. Body weights of virus-infected (n = 8) animals were monitored daily for 3 days. Body weights of virus-infected (n = 4) animals were monitored daily for 6 days. Data are presented as the mean percentages of the starting weight (±SD). (D) Number of genomic mutation types detected in viruses grown in Syrian hamster lung. RNA was extracted from the virus in lung homogenates from the Day 6 post-infection Syrian hamsters, and RNA sequencing was performed. Mutations with a read depth of at least 1000x and an allele frequency of at least 0.5% were compared between the wild-type and mutant viruses. Mean values compared by using an unpaired Student's t test ($^{**}P<0.01$). (E) SARS-CoV-2 genome organization and genomic locations of synonymous or nonsynonymous substitutions detected in the genomes of viruses grown in hamster lungs. The different directions of the triangles indicate each of the four individual hamsters. The number of nucleotide changes in viruses grown in Syrian hamster lung. The number of nucleotide changes, detected as synonymous and nonsynonymous substitutions, at a read depth of at least 1000x and an allele frequency of >0.5% were compared between the wild-type and nsp14-P203L mutant viruses.

710 Table 1. Amino acid sequence of nsp14 in SARS-CoV-2 epidemic strains.

Appearance frequency ranking	Substitution in nsp14	Number of sequences	Frequency of appearance (%)
1	–	25913	92.27
2	A320V	192	0.68
3	F233L	144	0.51
4	S374A	123	0.44
5	L177F	116	0.41
6	T250I	61	0.22
7	F377L	51	0.18
8	A138V	39	0.14
9	V120A	35	0.12
10	T16I	34	0.12
11	S369F	33	0.12
12	G481S	31	0.11
13	M501I	28	0.10
13	D345G	28	0.10
13	N129D	28	0.10
16	P203L	26	0.09
16	L177F, T372I	26	0.09
18	P297S	25	0.09
18	T31I	25	0.09
20	D324Y	24	0.09

711 28,082 sequences that were annotated as Human and free of undetermined or mixed nucleotides were used in
712 the analysis. Amino acid substitutions were defined as a change relative to the hCoV-19/Wuhan/Hu-1/2019
713 reference sequence. —, no mutation was found compared with the reference sequence.

714 Table 2. Nucleotide mutation rates of SARS-CoV-2 with different nsp14 variants.

Ranking of nsp14	Substitution in nsp14	Number of comparison sequences	Substitution rate per year in	
			whole genome	S+M+E gene
1	–	25471	19.8	4.31
5	L177F	114	27.3	7.45
7	F377L	51	13.0	2.81
11	S369F	33	26.2	2.48
13	M501I	28	21.9	3.07
16	P203L	24	35.9	5.29
17	L177F, T372I	26	59.8	9.82
18	P297S	25	17.1	2.48

715 The number of mismatched nucleotides in the alignment of the reference sequence with the comparison
716 sequence of each group was counted, and the average value was calculated. hCoV-19/Wuhan/Hu-1/2019 was
717 selected as the reference sequence. — , no mutation was found compared with the
718 hCoV-19/Wuhan/Hu-1/2019 sequence.

719 Table 3. Nucleotide mutation rates of the seven nsp14 variants for each cluster in which the maximum number
720 was observed

Ranking of nsp14	Substitution in nsp14	Lineage (PANGO ID)	Number of comparison sequences	Substitution rate per year in the whole genome
5	L177F	B.1.1.25	54	7.8
7	F377L	B	50	8.5
11	S369F	B.1.1	17	13.4
13	M501I	B.1	11	4.4
16	P203L	B.1.1.33	6	58.8
		B.1	6	28.0
17	L177F, T372I	B.1.113	20	50.1
18	P297S	B.4	11	16.1

721 The number of mismatched nucleotides in the alignment of the reference sequence with the comparison
722 sequence of each group was counted, and the average value was calculated. hCoV-19/Wuhan/Hu-1/2019 was
723 selected as the reference sequence. A scatter plot of these nsp14 is shown in Fig 4B and Supplementary fig 4.
724
725
726

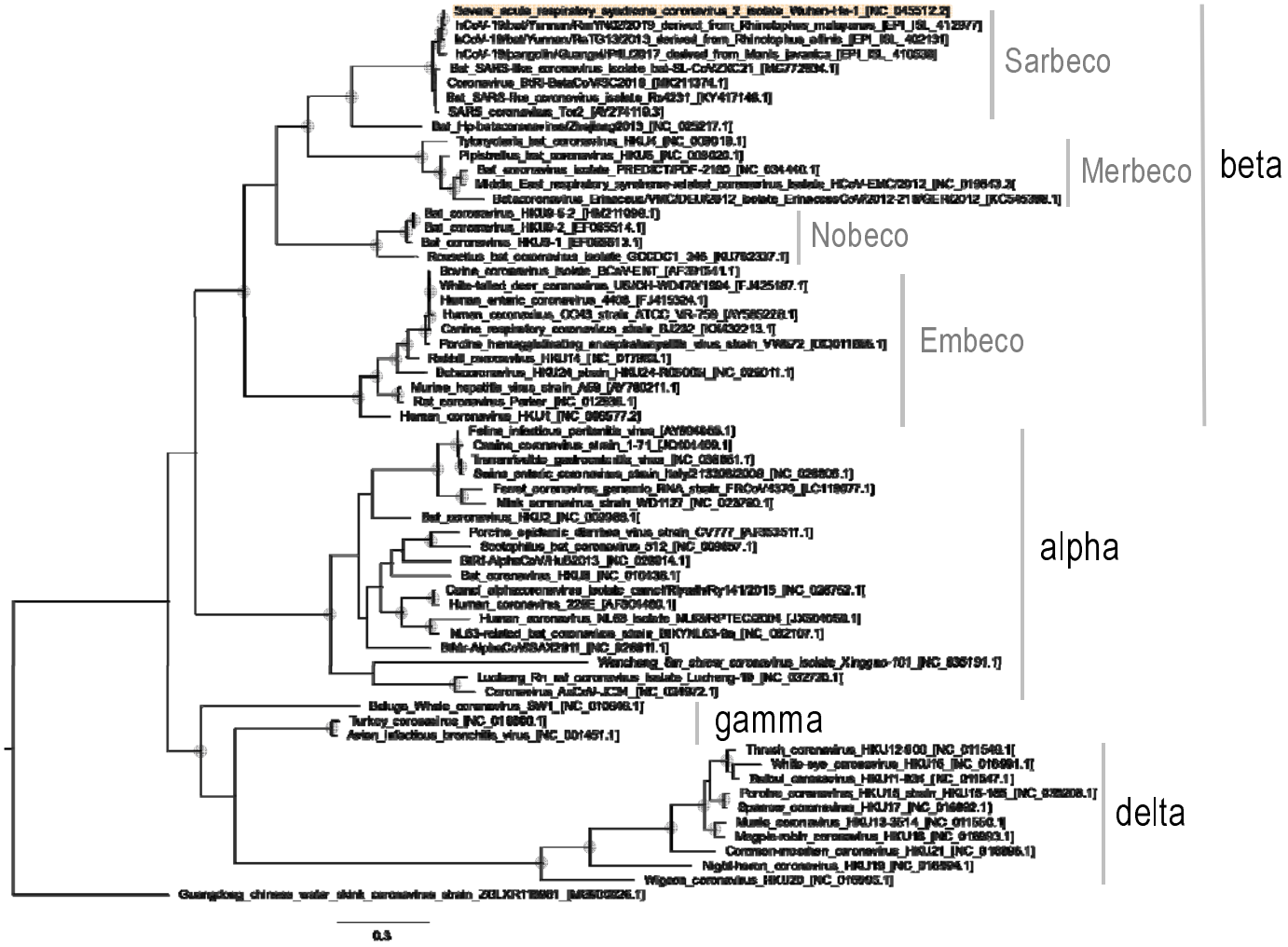

Fig. 1

(A)

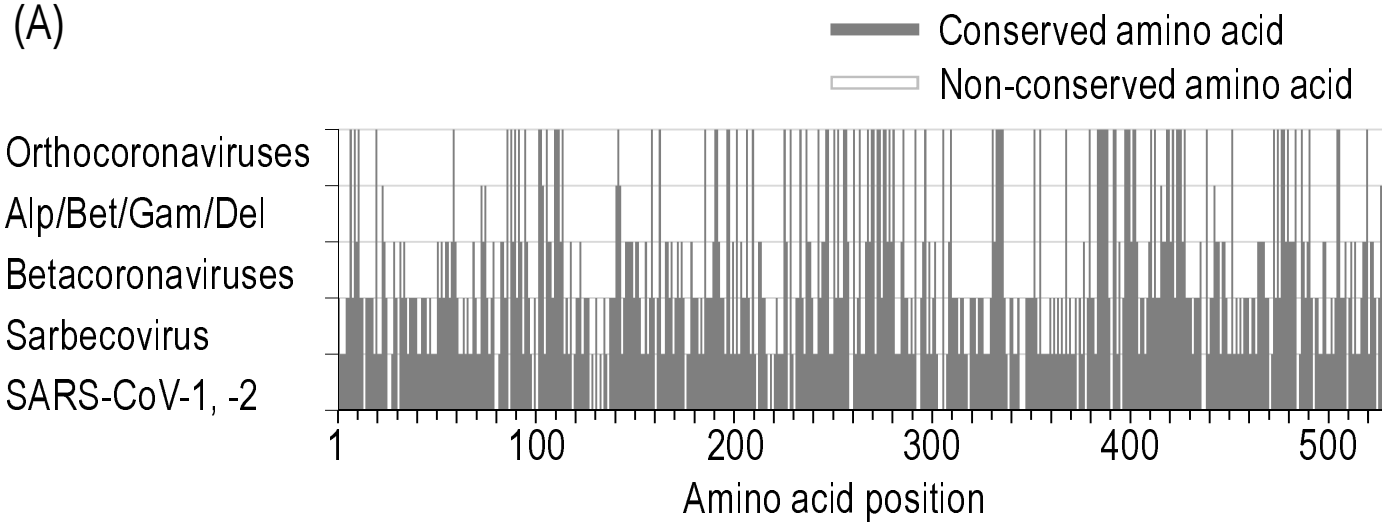
Conserved amino acid
Non-conserved amino acid
Orthocoronaviruses
Alp/Bet/Gam/Del
Betacoronaviruses
Sarbecovirus
SARS-CoV-1, -2
1
100
200
300
400
500
Amino acid position

(B)

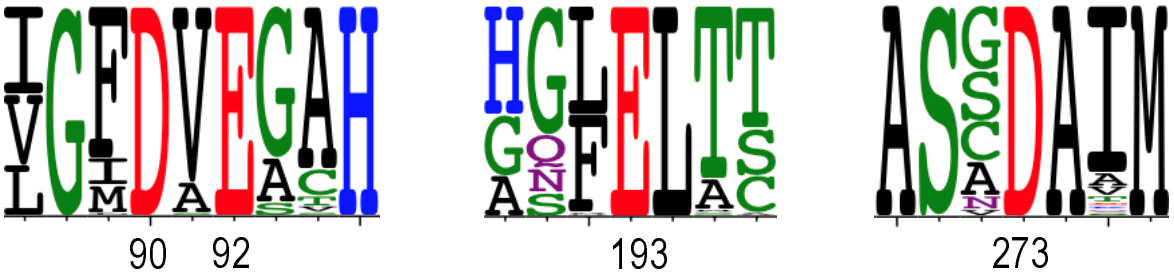
90
92
193
273

Fig. 2

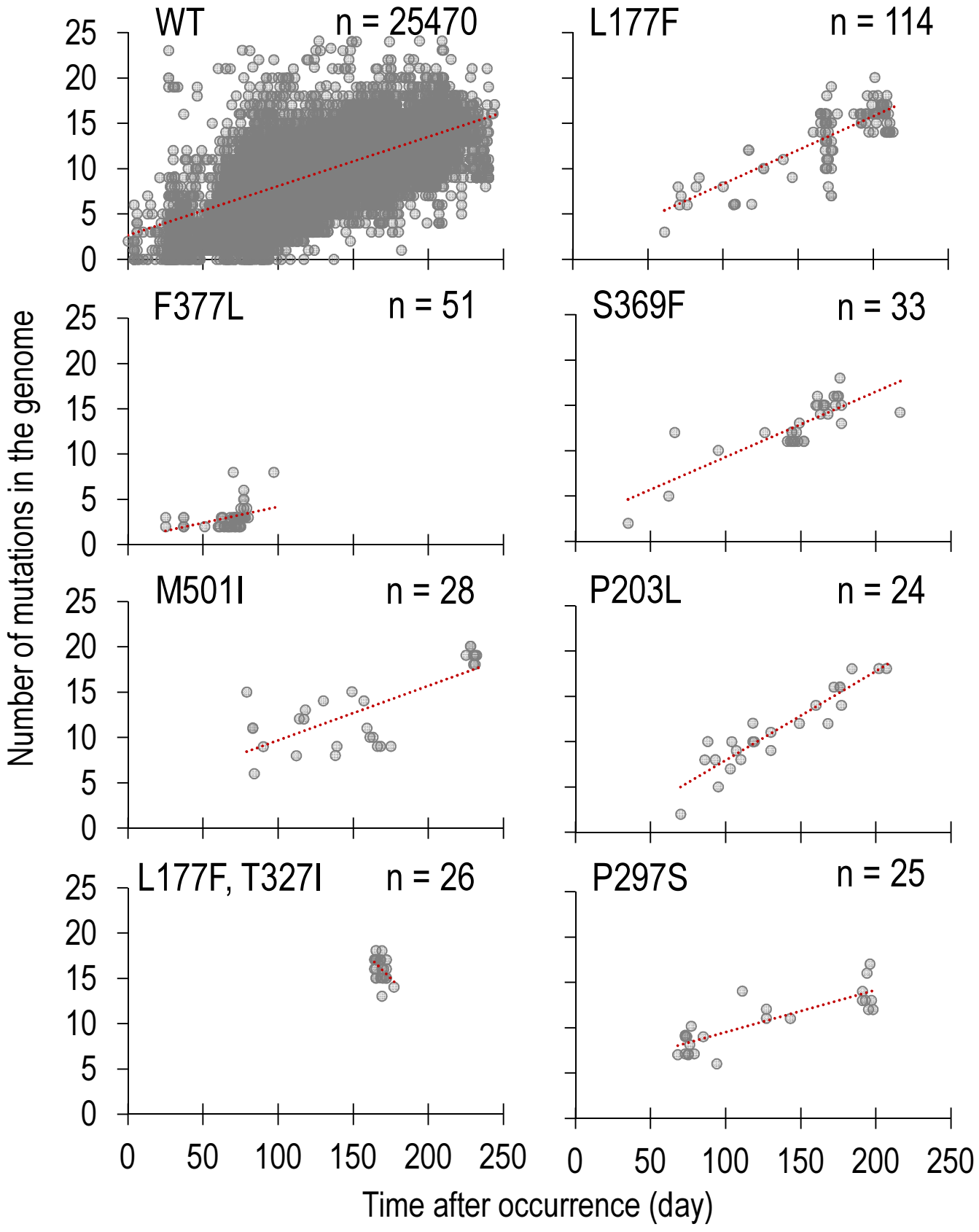
WT
n = 25470
L177F
n = 114
F377L
n = 51
S369F
n = 33
M501I
n = 28
P203L
n = 24
L177F, T327I
n = 26
P297S
n = 25
Number of mutations in the genome
Time after occurrence (day)
0
5
10
15
20
25
0
50
100
150
200
250

Fig. 3

(A)

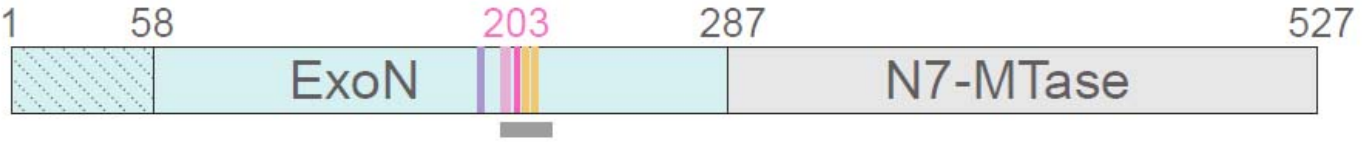

(B)

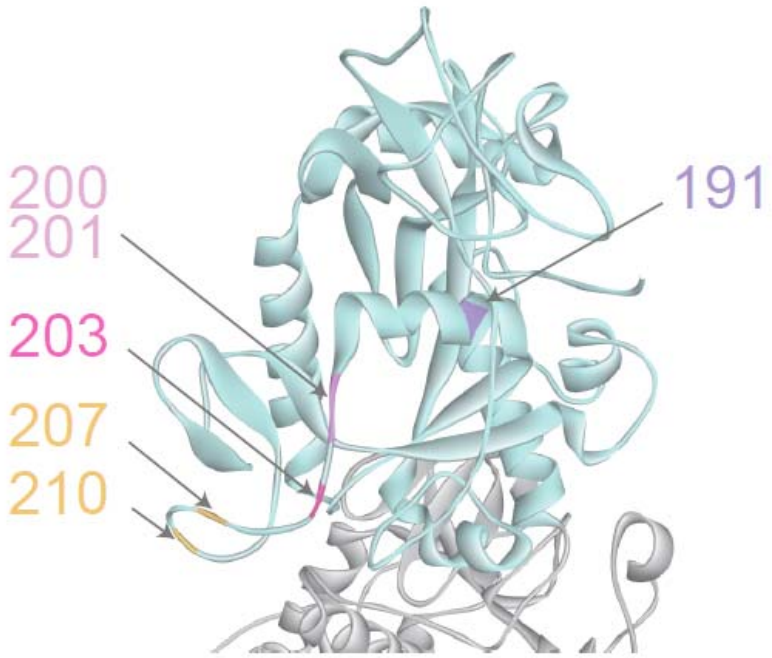

Fig. 4

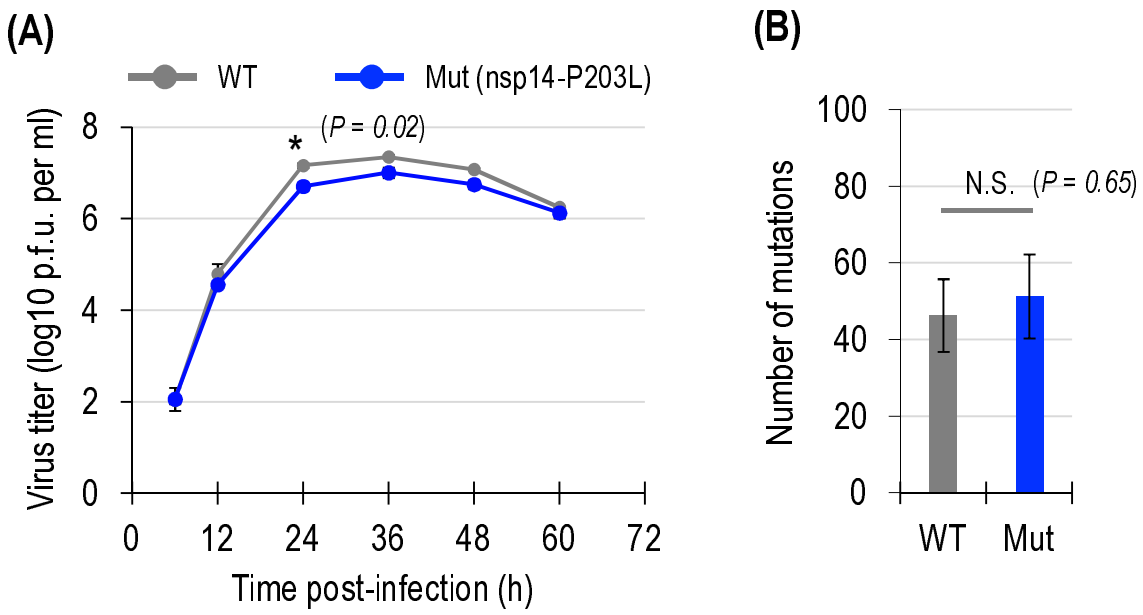
(A)
WT
Mut (nsp14-P203L)
(P = 0.02)
*
Virus titer (log10 p.f.u. per ml)
8
6
4
2
0
0
12
24
36
48
60
72
Time post-infection (h)
(B)
Number of mutations
100
80
60
40
20
0
N.S. (P = 0.65)
WT
Mut

Fig. 5

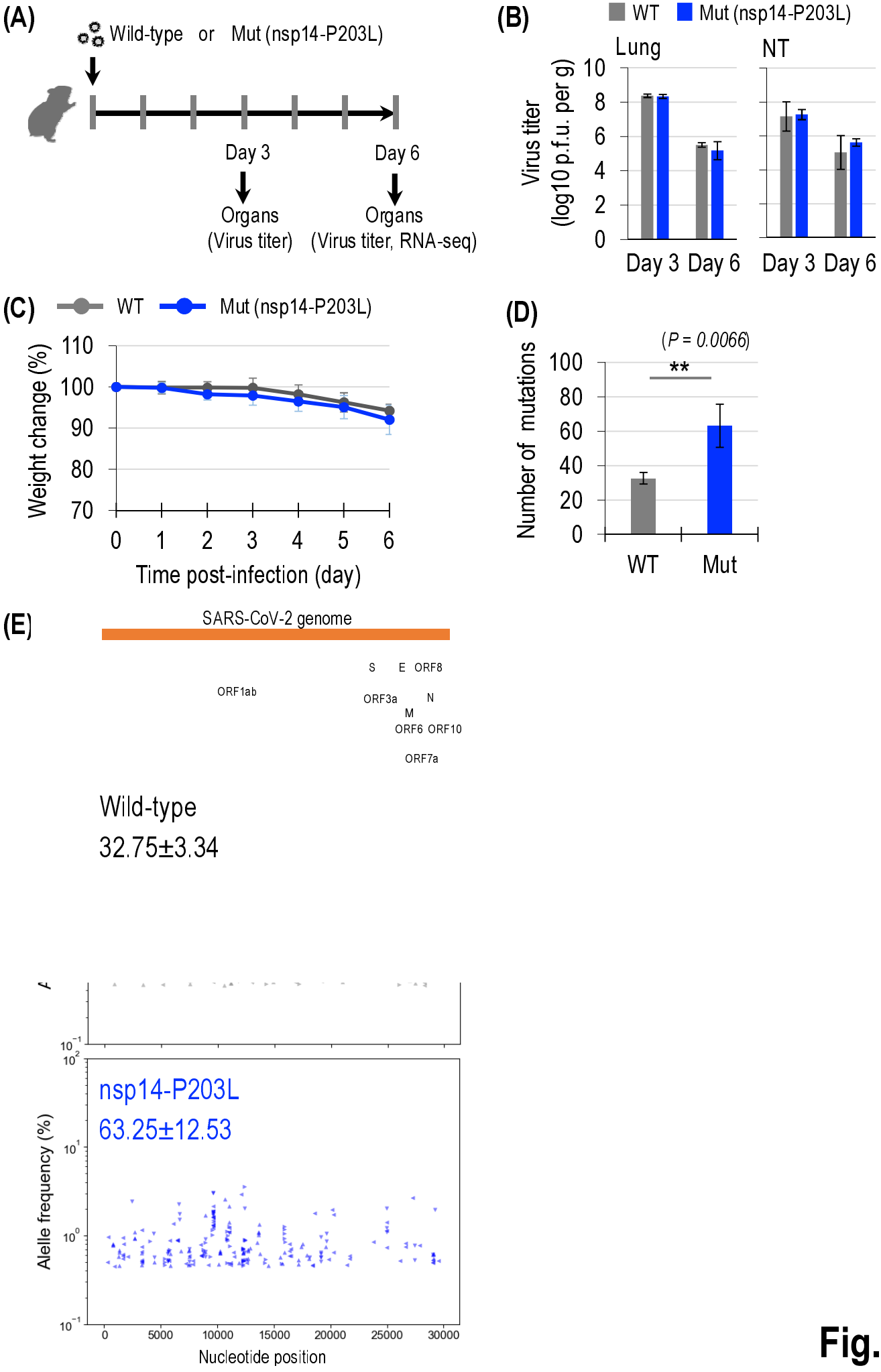
(A)
Wild-type or Mut (nsp14-P203L)
Day 3
Day 6
Organs
(Virus titer)
Organs
(Virus titer, RNA-seq)
(B)
WT
Mut (nsp14-P203L)
Lung
NT
Virus titer
(log10 p.f.u. per g)
Day 3 Day 6
Day 3 Day 6
(C)
WT
Mut (nsp14-P203L)
Weight change (%)
Time post-infection (day)
(D)
(P = 0.0066)
**
Number of mutations
WT
Mut
(E)
SARS-CoV-2 genome
ORF1ab
S
E
ORF8
ORF3a
N
M
ORF6
ORF10
ORF7a
Wild-type
32.75±3.34
nsp14-P203L
63.25±12.53
Alelle frequency (%)
Nucleotide position

Fig. 6